A magnetohydrodynamic stability study of reverse shear equilibria in the Tokamak Fusion Test Reactor

M. W. Phillips, M. C. Zarnstorff, J. Manickam, F. M. Levinton, and M. H. Hughes

Citation: Physics of Plasmas **3**, 1673 (1996); doi: 10.1063/1.871687
View online: http://dx.doi.org/10.1063/1.871687
View Table of Contents: http://scitation.aip.org/content/aip/journal/pop/3/5?ver=pdfcov
Published by the AIP Publishing

A magnetohydrodynamic stability study of reverse shear equilibria in the Tokamak Fusion Test Reactor

M. W. Phillips[a)]
Northrop Grumman, 4 Independence Way, Princeton, New Jersey 08540-6634

M. C. Zarnstorff and J. Manickam
Plasma Physics Laboratory, Princeton University, P.O. Box 451, Princeton, New Jersey 08543-0451

F. M. Levinton
Fusion Physics and Technology, Inc., 3547 Voyager St., Torrance, California 90503-1673

M. H. Hughes
Northrop Grumman, 4 Independence Way, Princeton, New Jersey 08540-6634

(Received 5 February 1996; accepted 19 February 1996)

A study is presented of the low-n ($n=1,2,3$) magnetohydrodynamic stability of equilibria with reverse shear safety factor profiles. The low-n stability boundaries are found to be characterized by resonance structures due to internal so-called ''infernal'' mode types of instabilities. The parametric dependence of shear reversal width and depth, current, and pressure gradient on the beta limit are determined by using profile models that allow each parameter to be varied independently. Reverse magnetic shear is found to have a stabilizing influence for modes with toroidal mode numbers $n \geqslant 2$ leading to the possibility of improved β limits in the Tokamak Fusion Test Reactor (TFTR) [Plasma Phys. Controlled Nucl. Fusion Res. **26**, 11 (1984)]. © *1996 American Institute of Physics.* [S1070-664X(96)03905-3]

I. INTRODUCTION

Recently, there has been renewed interest in a mode of tokamak operation characterized by nonmonotonic q profiles. This interest has been motivated by recent experiments, theoretical calculations, and progress in tokamak design. Initially, interest in reverse shear profiles in tokamaks resulted from the recognition that very small or even reversed shear permits access to the second stable region for ballooning modes. This allows the pressure profile to be strongly peaked in the center maximizing the achievable beta. Both DIII-D[1] and Joint European Torus (JET)[2] demonstrated experimentally that plasmas with reversed shear q profiles could be produced and sustained for a significant length of time at high temperature (the q profile evolves, however).[3,4] In addition, results from these experiments suggested that such a mode of operation could lead to significantly enhanced confinement. Further interest in reversed shear plasmas was sparked during the design of the TPX tokamak,[5] which was intended as a steady-state machine. A steady-state tokamak where the diffusion-driven (bootstrap) current drives most of the plasma current is desirable since it relaxes the requirements for external current drive systems and recirculating power. The resulting current distribution in a primarily bootstrap current-driven plasma tends to be hollow, resulting in a reversed shear q profile. Theoretical studies of such configurations[6,7] have found them to be as robust, from a magnetohydrodynamic (MHD) stability standpoint, as the more conventional monotonic current profiles.

Interest in the reverse shear mode of operation prompted an investigation of this mode of operation in the Tokamak Fusion Test Reactor (TFTR).[8,9] Findings suggest that reversed shear q profiles can lead to a new enhanced mode of confinement characterized by very low particle and thermal transport. This confinement regime has been termed the ''Enhanced Reverse Shear'' (ERS) mode.[10] A characteristic of the experiment thus far is that a hollow current profile is formed with highly reversed shear that relaxes as the plasma evolves. Both the minimum value of q and the amount of shear reversal, $\Delta q = q_0 - q_{\min}$, decrease during the experiment. For sufficiently high beta when $q_{\min}$ drops to a value $q_{\min} \sim 2$, a hard stability limit is encountered due to a low-n instability. Characterizing this stability limit and mapping out the stable operating regime for TFTR is the motivation for the present study. The purpose of this study is to parametrize the stability limitations due to low-n ($n=1$, 2 and 3) MHD modes for TFTR equilibria with reverse shear q profiles. An important advance aiding the analysis of the experiments has been the development of the motional Stark effect (MSE)[11,12] diagnostic for measuring the q profile. This allows a direct measurement of the q profile, which heretofore was a large uncertainty in comparing stability computations with experimental observation.

II. COMPUTATIONAL MODEL

Here we shall confine our interest to those equilibria characterized by q profiles, with a single minimum occurring at some location between the magnetic axis and plasma edge. For these profiles a region of shear reversal occurs in the central region of the plasma. The essential parameters characterizing the q profile are the value q_0 on axis, the minimum value of $q, q_{\min}$, the radial location of the minimum surface, and the value q_{edge} at the plasma surface. It is of interest to systematically study the effect of each of these parameters independently on low-n stability. This demands a

a)Electronic mail: phillips@grump.com

carefully defined procedure for prescribing the q profile when calculating MHD equilibria. The steady-state equilibria derived from experimental measurements are such that the current density is small or zero at the plasma edge. Arbitrarily chosen q profiles, however, often result in unrealistic current distributions near the boundary. A common remedy for this problem is to specify a form of the current profile, such as $\langle \mathbf{J}\cdot\mathbf{B}\rangle/\langle \mathbf{B}\cdot\nabla\phi\rangle$ or $\langle J_\phi\rangle$, that can be tailored so that current reduces smoothly to zero at the boundary. Here $\langle\ \rangle$ denotes the flux surface average. A disadvantage of using current profiles in the present context is the difficulty in retaining adequate control over all the parameters of interest. For example, simply changing β would cause both q_0 and $q_{\rm edge}$ to vary. Since we are interested here in controlling several characteristics of the q profile simultaneously, this difficulty is compounded. A procedure described below, however, was found to adequately satisfy our requirements.

To circumvent the problem of specifying the q profile and current profile characteristics simultaneously, we choose a hybrid method in which the safety factor profile is specified but a free parameter is left over in order to control the current profile at the edge. This free parameter is chosen iteratively by the equilibrium code to keep the poloidal current equal to zero. We use the conventional notation whereby the magnetic field is given by $\mathbf{B}=\nabla\phi\times\nabla\psi+g\ \nabla\phi$, where ψ is the poloidal flux function and (r,ϕ,z) are cylindrical coordinates. The condition of zero poloidal current is equivalent to specifying $g'=0$, where the prime denotes the derivative with respect to ψ. We also choose $p'=0$ on the plasma edge. These two conditions make $j_\phi=-rp'-gg'/r=0$ at the plasma edge as well.

Equilibria for this study were computed using the EQGRUM3 equilibrium code. This is a fixed boundary code that solves for the Grad–Shafranov equation for the inverse equilibria $r(\psi,\phi)$ and $z(\psi,\theta)$. The code is similar to other inverse equilibrium solvers,[13] although the specific numerical implementation is quite different. In particular, EQGRUM3 uses a fast multigrid[14] solver, which allows it to compute high resolution equilibria. The code is also capable of computing anisotropic equilibria, although this feature is not used for this study. The model safety profile was chosen to be as simple as possible yet still have all the features of the reverse shear profiles measured experimentally in TFTR. The q profile is specified in two parts—an inner and outer portion. The inner part specifies q from the magnetic axis to the minimum q location and the outer part specifies q from the minimum q location to the plasma edge. The inner part of the q profile is defined by

$$q(\bar{\psi})=q_0+(q_{\rm min}-q_0)[2-\bar{\psi}+c_0(1-2\bar{\psi}+\bar{\psi}^2)]\bar{\psi}, \quad (1)$$

where

$$\bar{\psi}=\frac{\psi-\psi_0}{\psi(q_{\rm min})-\psi_0}$$

and

$$c_0=1+\frac{(q_{\rm edge}-q_{\rm min})\psi_{\rm min}^2}{(q_{\rm min}-q_0)(1-\psi_{\rm min})^2}, \quad \text{for } \psi_0\leqslant\psi\leqslant\psi_{\rm min}.$$

The outer part is prescribed by

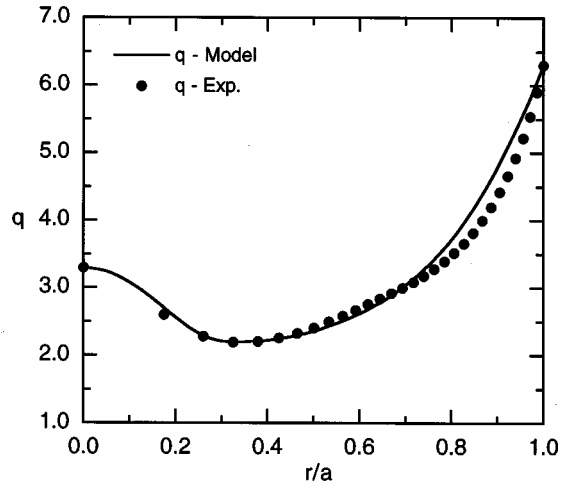

FIG. 1. Model safety factor profile, q, compared to a measured reverse shear q profile in TFTR from shot #83998 at $t=2.99$ s.

$$q(\bar{\psi})=q_{\rm min}+(q_{\rm edge}-q_{\rm min})[(1-\bar{\psi})\bar{\psi}^2+\bar{\psi}^{\alpha_q}], \quad (2)$$

where

$$\bar{\psi}=\frac{\psi-\psi_{\rm min}}{\psi_{\rm edge}-\psi_{\rm min}}, \quad \text{for } \psi_{\rm min}\leqslant\psi\leqslant\psi_{\rm edge}.$$

Here ψ_0 is the value of ψ on the magnetic axis, $\psi_{\rm edge}$ is the value of ψ on the plasma surface, and $\psi_{\rm min}$ is ψ at $q_{\rm min}$. The inner and outer profiles match q, q', and q'' at $\psi_{\rm min}$. A comparison between the model safety factor profile and an experimentally observed safety factor profile is shown in Fig. 1. The parameter α_q is the free parameter chosen by the equilibrium code to make the poloidal current equal to zero, and generally has a value in the range 3.5–4.75. A consequence of the choice to specify the relative poloidal flux value at which q is a minimum is that as $q_{\rm min}$ and β are varied the radius at which q is a minimum also changes. This change, however, tends to be small. As an example, for the case when $q_{\rm edge}=6.3$, $q_0=q_{\rm min}+1$, with β at the low-n marginal stability point, $r_{\rm min}/a=0.325$ for $q_{\rm min}=1.1$ and $r_{\rm min}/a=0.363$ for $q_{\rm min}=2.5$. Examples of the $\langle \mathbf{J}\cdot\mathbf{B}\rangle/\langle \mathbf{B}\cdot\nabla\phi\rangle$ profile resulting from this q profile specification are shown Fig. 2. As noted above, q profiles often have unrealistic current profiles near the edge. This is typically manifested by values $\langle \mathbf{J}\cdot\mathbf{B}\rangle/\langle \mathbf{B}\cdot\nabla\phi\rangle$ at the edge that depart considerably from zero, or by a region where $\langle \mathbf{J}\cdot\mathbf{B}\rangle/\langle \mathbf{B}\cdot\nabla\phi\rangle$ is negative. As shown in Fig. 2 this q profile specification results in $\langle \mathbf{J}\cdot\mathbf{B}\rangle/\langle \mathbf{B}\cdot\nabla\phi\rangle$ equal to zero at the edge. For the case $q_{\rm min}=1.1$ the $\langle \mathbf{J}\cdot\mathbf{B}\rangle/\langle \mathbf{B}\cdot\nabla\phi\rangle$ profile has a region near the edge, where it is slightly negative. Transport analysis of high-current ''supershot'' plasmas[9] frequently show the $\langle \mathbf{J}\cdot\mathbf{B}\rangle/\langle \mathbf{B}\cdot\nabla\phi\rangle$ to be near zero in the outer edge of the plasma, with the current channel located primarily in the center.[15] Our prescription for specifying q models this feature adequately. It should be noted that while the above q profile prescription works well in circular geometry such as TFTR, it generates a q profile with two minima in elongated ''D''-shaped plasmas.

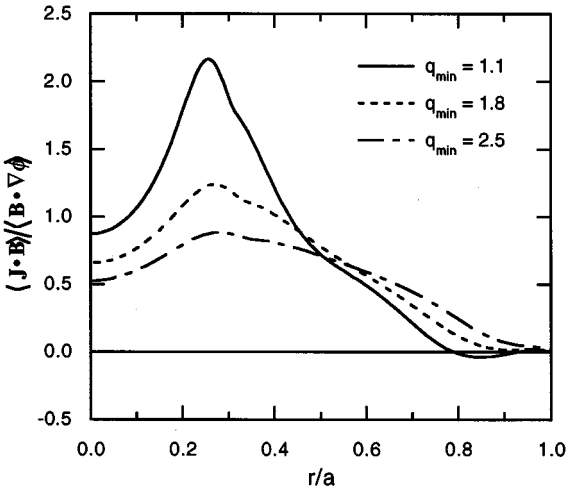

FIG. 2. The $\langle \mathbf{J}\cdot\mathbf{B}\rangle/\langle \mathbf{B}\cdot\nabla\phi\rangle$ profiles resulting from the model safety factor profile for several values of the minimum q value, $q_{\min}$.

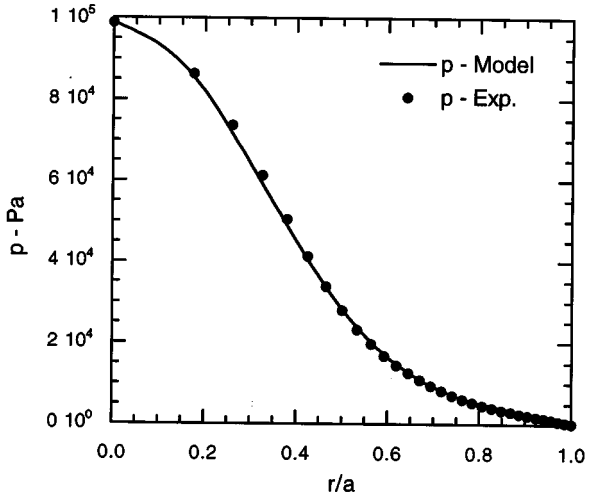

FIG. 3. Model pressure profile, p, compared with TRANSP modeling of TFTR experimental data from shot #83998 at $t=2.99$ s.

A simple formula for the pressure profile was chosen that closely models TFTR supershot pressure distributions. A typical supershot pressure profile is highly peaked on axis and decays exponentially as a function of ψ, except near the edge of the plasma. The pressure profile model is prescribed by

$$p(\psi)=p_0 e^{-\alpha_1 \bar{\psi}}(1-\bar{\psi}^{\alpha_0})^2. \tag{3}$$

Here the poloidal flux label, $\bar{\psi}$, is normalized to have a value of zero at the magnetic axis and unity at the plasma edge. For typical supershots the parameter α_1 has the range $2.5\leqslant\alpha_1<4$. This form of the pressure profile has essentially two features. First, is an exponentially decaying function of ψ over the innermost 80% of the plasma. This usually matches supershot data very accurately. The second part of Eq. (3) forces both p and p' to smoothly tend to zero at the plasma edge for an α_0 in the range $10\leqslant\alpha_0\leqslant 20$. The central pressure p_0 is adjusted to change the value of β. A comparison of the model with a pressure profile computed from a transport analysis of the reverse shear experiment in TFTR (shot #83998) is shown in Fig. 3. It should be noted that shot #83998 does not have the so-called "Enhanced Reverse Shear" (ERS) mode.[10] Reverse shear plasmas in TFTR come in two verities: plasmas with confinement similar to supershots and Enhanced Reverse Shear shots with significantly enhanced confinement in the core of the plasma. Shots that enter ERS mode develop a quite different pressure profile that is more highly peaked in the center. Non-ERS shots have pressure profiles similar to supershots.

The equilibria for these studies were computed on a grid of 129 radial surfaces and 320 poloidal nodes. The estimated maximum truncation error due to the finite size grid is less than 3×10^{-4} when compared with the fully converged solution. As the limiting β for ideal MHD stability is approached from above, the radial derivatives at mode rational surfaces tend to become very steep. To accurately represent this computationally in the stability codes a finer mesh is used than by the equilibrium solver. This is accomplished by mapping the equilibria to a larger number of radial surfaces using a separate mapping code.

The ideal MHD stability analysis was performed using the KOSMIK low-n stability code. This code was originally designed to compute the low-n number stability of anisotropic plasmas using the Kruskal–Oberman energy principle[16] (hence the KOS in the name stands for Kruskal–Oberman Stability). For computations described here, parts of the code were adapted to solve the isotropic, incompressible MHD equations. In this version of the code the MHD equations are written in terms of a vector streamfunction $\mathbf{u}$, such that $\mathbf{v}=\nabla\times\mathbf{u}$, where $\mathbf{v}$ is the perturbed fluid velocity. The formulation is similar to the ARES code[17] design, except a different gauge transformation is used, such that $u_\phi=0$. Although this choice of gauge precludes the case where the toroidal mode number, $n=0$, it simplifies the matching of the vacuum solution at the plasma surface. The KOSMIK code can also model the vacuum region between the plasma and a conducting boundary and has the capability of modeling multiple, perfectly conducting surfaces. Most of the ideal MHD computations presented here invoked a "wall at infinity" boundary condition (i.e., no external conducting surfaces), except where otherwise noted. This boundary condition generally gives the most pessimistic stability criteria. The code has been benchmarked against the ARES code, and several specific reverse shear cases were compared in detail using the two codes. When numerically converged, solutions from both codes are found to be in excellent agreement.

III. NUMERICAL RESULTS

The prototype of the equilibria modeled here was taken from shot #83998 at $t=2.99$ s. This particular shot was chosen because it had good quality diagnostic data, including MSE measurements from which the q profile was derived. It did not, however, enter the so-called Enhanced Reverse Shear (ERS) mode, where the particle transport is observed to be reduced by a large factor. There was MHD activity that

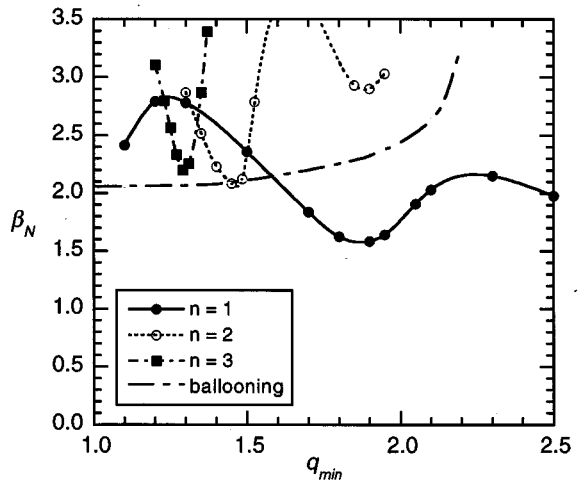

FIG. 4. Normalized beta limits for the $n=1,2,3$, and ballooning instabilities as a function of the minimum q value, $q_{\min}$. For these cases $q_{\text{edge}}=6.3$, $\Delta q=q_0-q_{\min}=1.0$, and $\alpha_p=4$.

appeared toward the end of the shot, which ultimately terminated with a disruption, typical of those observed on other reversed shear shots. The geometrical parameters for the equilibria in this study are $R=2.59$, $a=0.92$, and $\epsilon=1.05$. This represents a plasma that almost fills the available cross section of TFTR and is typical of reversed shear equilibria. For shot #83998 at $t=2.99$ s the equilibrium had $q_{\text{edge}}=6.3$, $q_0=3.2$, and $q_{\min}=2.2$, with the minimum located at $\psi_{\min}=0.15$. The corresponding pressure profile parameters were $\alpha_1=4$ and $\alpha_0=20$.

Typically, $q_{\min}$ decreases during the course of the experiment until it reaches a value ~ 2.0, when a low-n instability appears. To gauge the effect of $q_{\min}$ on the beta limit, $q_{\min}$ was varied and the critical beta for marginal stability was computed for the $n=1$, 2, and 3 modes as well as the ballooning mode. The result is shown in Fig. 4, which plots the normalized beta, $\beta_N=\beta_r/[I(\text{MA})/a(\text{m})B(\text{T})]$, as a function of $q_{\min}$. For this calculation the difference between the central and minimum values of q value, Δq, was kept fixed at 1 (i.e., $\Delta q=q_0-q_{\min}=1$). The remaining parameters were chosen to reflect shot #83998 at $t=2.99$ s. The minimum value of q was found to have an important influence on the critical beta limit. The beta limit drops abruptly when $q_{\min}$ is just below a rational value. For the $n=1$ mode this feature is due to an instability where the poloidal mode number $m=2$ is the dominant harmonic. The mode structure of the $n=1$ is a combination of internal instability, with a significant external component. In contrast, the $n=2$ and $n=3$ modes had little external component and are essentially internal modes. These modes can be classified as ''infernal'' modes[18] similar to that found in low shear plasmas. Figure 5 shows the mode structure of the instabilities for (a) $n=1$, (b) $n=2$, and (c) $n=3$ just inside the unstable region at the point, where the β limit is smallest for each mode number. The dip in beta normal for the $n=1$ mode near $q_{\min}=2$ offers an explanation for the stability boundary observed in the experiment. During the experiment $q_{\min}$ slowly decreases as current penetrates into the center of the plasma. Near $q_{\min}=2$ the beta is sufficiently high that the resonance structure of the $n=1$ mode is encountered, leading to instability and subsequent disruption.

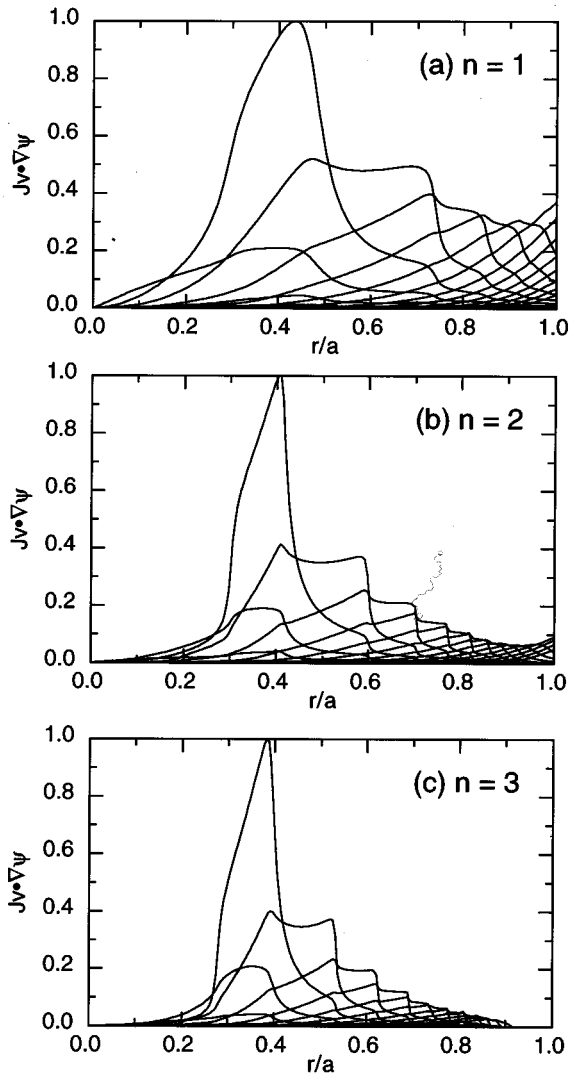

FIG. 5. Radial component of the perturbed velocity just inside the ideal instability threshold for (a) $n=1$, $q_{\min}=1.9$; (b) $n=2$, $q_{\min}=1.475$; (c) $n=3$, $q_{\min}=1.3$.

The effect of changing the value of q on the surface of the plasma, q_{edge}, and hence the total current, is illustrated in Fig. 6 for the $n=1$ mode. The essential features of the stability diagram, namely, the lower beta limits at resonant surfaces, remain the same. Indeed, this feature is typical of all reverse shear equilibria. As shown in Fig. 6, when the plasma current increases, the normalized beta decreases only slightly for $q_{\min}<2$. The beta limit, thus, appears to be a beta normal limit. Above $q_{\min}>2$ the difference is somewhat larger. This is due to the broadening of the current profile, which tends to decrease the stability limit for external modes. The current profile is broadened both by the decrease in q_{edge} and the increasing $q_{\min}$, which redistributes the current to the outside. As a consequence for $q_{\min}>2$ the $n=1$ mode has a larger external component.

The form of the pressure distribution has a significant effect on the stability of the infernal mode. Figure 7 shows the stability boundaries as a function of $q_{\min}$ for several pres-

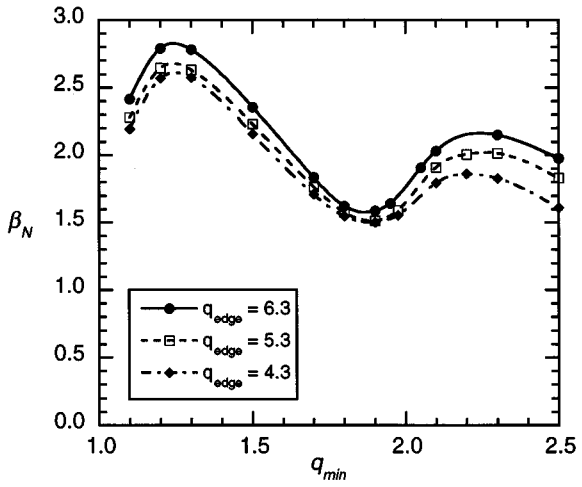

FIG. 6. The normalized beta limits for the $n=1$ instability as a function of the minimum q value for different q_{edge} values.

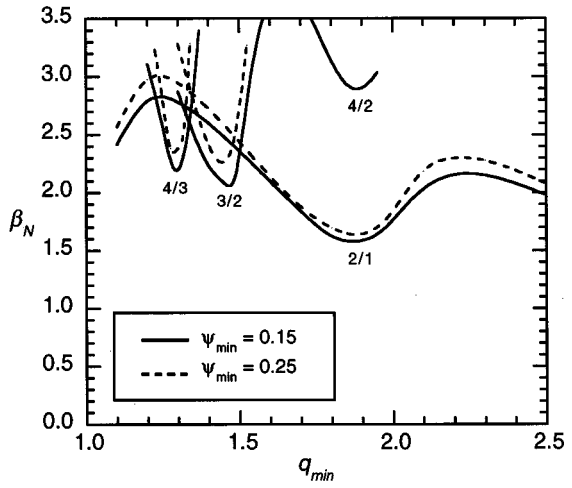

FIG. 8. The effect of shear reversal radius on the normalized beta limits for the $n=1$, 2, and 3 instabilities as a function of the minimum q.

sure peaking factors $p_0/\langle p\rangle$, where p_0 is the central pressure and $\langle p\rangle$ is the volume-averaged pressure. The pressure distribution in TFTR for reverse shear plasmas are similar to supershots for non-ERS plasmas with $p_0/\langle p\rangle \sim 5$ and somewhat more peaked for ERS plasmas with $p_0/\langle p\rangle \sim 7$. As the pressure distribution broadens (lower $p_0/\langle p\rangle$ or α_1) there is an increase in the normal beta limit. There appears to be a limit, however, to how broad the pressure profile can be made and still achieve this effect. Although not shown in Fig. 7, there is little overall increase in the beta limit for $\alpha_1=2$ compared to $\alpha_1=3$. Indeed, for the $\alpha_1=2$ case the nature of the instability limiting beta changes becoming more of an external kink mode with the effect of the resonance at $q_{\min}=2$ barely detectable.

So far the stability of reversed shear profiles is similar, in many respects, to previous studies of supershots with monotonic q profiles.[19] In both cases the infernal mode causes a decrease in the beta limit when $q_{\min}$ (or the central value q_0 in the case of monotonic profiles) is near a rational value. One difference is that the beta limit due to higher n number modes ($n \geqslant 2$) is somewhat higher then that computed for monotonic profiles. Of interest is whether increasing the amount of reverse shear increases stability. The two parameters of interest are the location of minimum shear $\psi_{\min}$ and $\Delta q = q_0 - q_{\min}$. The first parameter determines the radial extent of the reverse shear and the second parameter to what degree shear is reversed. Figure 8 demonstrates what occurs when the position of the inversion radius is increased. Overall the effect tends to be somewhat stabilizing. The increase in the minimum beta limit associated with the mode rational surfaces tends to be somewhat larger for the higher-n modes than for the $n=1$ mode. Changing $\psi_{\min}=0.15$ to $\psi_{\min}=0.25$ causes the relative minor radius to move out about 0.1. Figure 9 shows the effect changing Δq has on the $n=1$, 2, and 3 stability boundaries. The stability boundaries for the cases $\Delta q=1$ and $\Delta q=0.1$ are shown. Increasing Δq tends to in-

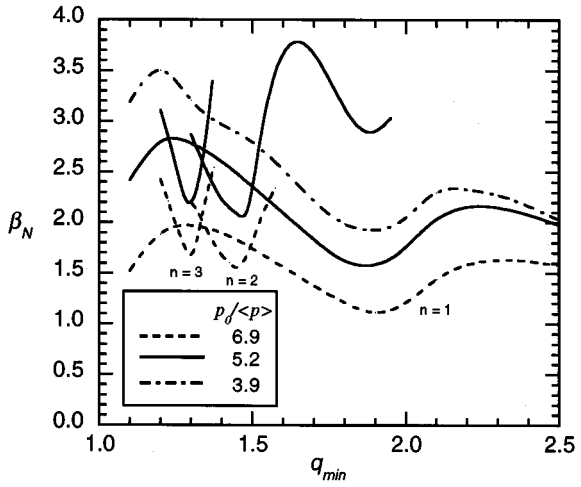

FIG. 7. The effect of pressure profile peaking on the normalized beta limits for the $n=1$, 2, and 3 modes as a function of the minimum q. Here $\alpha_1=3$, resulting in $p_0/\langle p\rangle=3.9$; $\alpha_1=4$, $p_0/\langle p\rangle=5.2$; and $\alpha_1=5$, $p_0/\langle p\rangle=6.9$.

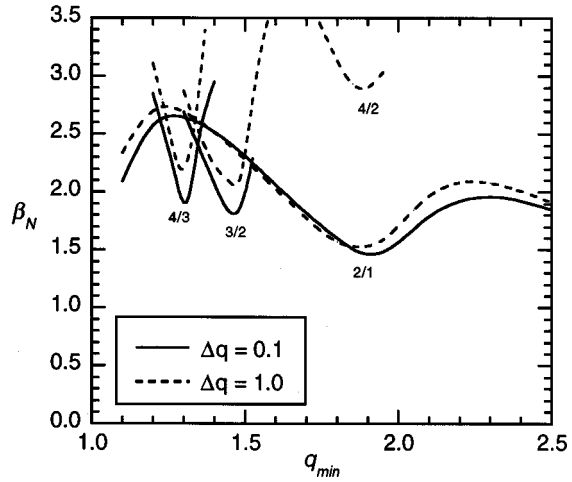

FIG. 9. The effect of shear depth on the normalized beta limits for the $n=1$, 2, and 3 instabilities as a function of the minimum q.

crease the normalized beta limits somewhat. Similar to the case of increasing the inversion radius, increasing Δq seems to have a larger effect on the $n=2$ and 3 modes than on the $n=1$ mode. Several cases were run to determine whether the effects are multiplicative. Increasing both Δq and shear reversal radius leads to proportionally higher beta limits.

IV. BALLOONING OPTIMIZED PROFILES

The cases considered so far all had pressure profiles similar to supershots. This pressure profile tends to be fairly optimal for ballooning stability when q is monotonic as is typical in supershots. The observation that the pressure profile assumes an optimal conforming shape when β is at the value predicted by the Troyon–Gruber scaling law[20] $\beta = g_T I(\mathrm{MA})/a(\mathrm{m})B(\mathrm{T})$, where $g_T \sim 3$, is similar to observations in other tokamak experiments.[21] The empirical Troyon–Gruber scaling law was determined using ballooning optimized profiles. A likely explanation why experimental pressure profiles tend to assume the optimum shape is that ballooning modes cause a local flattening of the pressure profile that changes the pressure gradient to be less than or equal to the critical pressure gradient for ballooning modes. The ballooning stability of reverse shear equilibria is quite different from monotonic profiles. In the reverse shear case the plasma has no ballooning limit in the region where shear is negative. Consequently the pressure profile can be more peaked in the central region, as indeed is the case of Enhanced Reverse Shear (ERS) plasmas. There is a slight dip in the critical pressure gradient when shear is positive yet still small. In the region where the q profile is monotonically increasing, the critical pressure gradient is essentially similar to the purely monotonic profile case.

Infernal modes, such as the $n=2$ and 3 are strongly influenced by the vicinity of the ballooning mode boundary. Low shear changes the ballooning mode ordering so that resonant low-n modes are more unstable than large-n modes,[22] however, the low-n modes are still dependent on the infinite-n ballooning boundary. In Fig. 4, the ballooning mode beta limit is reached before the $n=1$ limit and the minimum of the $n=2$ and 3 beta limits lie very close to the ballooning mode stability boundary. If the profiles are adjusted to maintain stability with respect to ballooning modes at higher beta, they would be expected to also be more stable to the lower-n modes as well. Figure 10 shows the pressure gradient typical of supershots and used in the study in the preceding section (solid line) at the $n=1$ marginal stability point and the first and second critical pressure gradients for the ballooning mode. It is clearly ballooning unstable just outside of the $q_{\min}$ flux surface. In addition, a model pressure profile that avoids the ballooning unstable region (dotted line) is also depicted in Fig. 10. The formula used for these pressure profiles is a generalization of Eq. (4):

$$p(\psi) = p_0 \left[\sum_i a \exp(-b_i \bar{\psi}^{c_i}) \right] (1-\bar{\psi}^{\alpha_0})^2. \tag{4}$$

In Fig. 10, for the dotted line $\alpha_0=10$, $a_1=0.5$, $b_1=-150$, $c_1=2.0$, $a_2=0.5$, $b_2=-3$, and $c_2=1.5$. For both equilibria $q_{\min}=1.2$, $\Delta q=1.0$, and $q_{\mathrm{edge}}=6.7$.

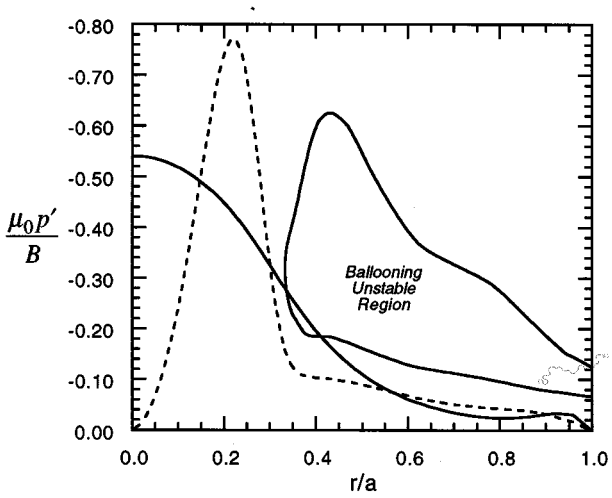

FIG. 10. The pressure gradient for a supershot-type pressure distribution (solid line) and a ballooning stable pressure distribution (dotted line) and the critical pressure gradient for ballooning modes. For both profiles $p_0/\langle p\rangle = 5.0$, $q_{\min}=1.2$, $\Delta q=1$, $q_{\mathrm{edge}}=6.7$, and $\beta_N=2.45$.

The normalized beta limit as a function of $q_{\min}$ is shown in Fig. 11 for the ballooning stable pressure profile depicted in Fig. 10. Two values of Δq are shown: a low shear case with $\Delta q=0.005$, and a higher shear reversal case with $\Delta q=1$. The q profiles outside the $q_{\min}$ surface are identical for both cases. As can be seen in Fig. 11, for the case where $\Delta q=1$, the $n=2$ and 3 stability limits are well above the $n=1$ stability limit. Equilibria with pressure profiles optimized for ballooning have much higher beta limits for $n \geqslant 2$ compared to nonoptimized pressure profiles where the minimum beta limit for the $n=2$ and 3 modes is always below the $n=1$ threshold. Infernal modes depend not only on beta but also depend on how flat the shear is, as can be seen in Fig. 11 for the $\Delta q=0.005$ case. Note, since the q profile is identical outside the $q_{\min}$ surface for both cases, the critical pressure gradients for ballooning are also the same for both cases. The

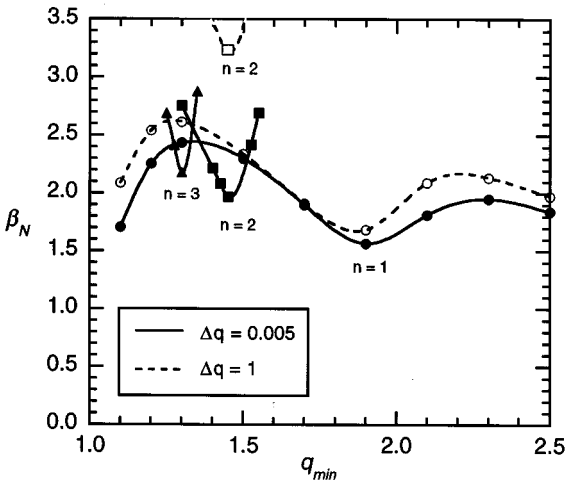

FIG. 11. Critical beta normal versus $q_{\min}$ for ballooning stable pressure profiles for $\Delta q=0.005$ (solid) and $\Delta q=1$ (dotted).

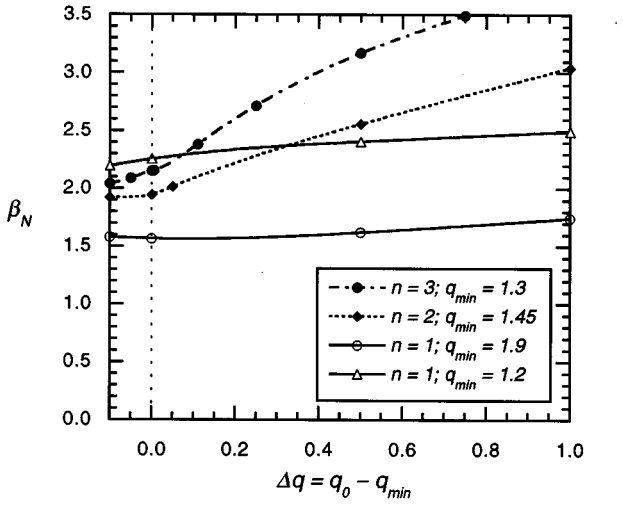

FIG. 12. Minimum critical beta normal as a function of Δq for the $n=1$, 2, and 3 modes for a ballooning stable pressure distribution.

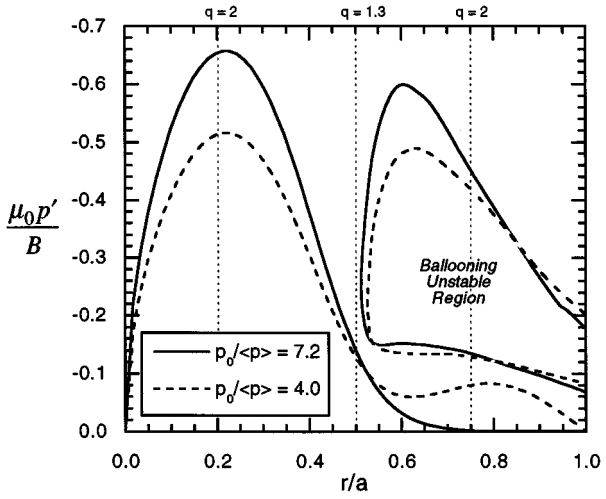

FIG. 13. Peaked and broad pressure gradient profiles and the corresponding critical pressure gradients at the marginally stable point for the $n=1$ mode.

beta limit of ballooning optimized profiles is much more sensitive than nonoptimized profiles to the amount of shear reversal. This can be seen by comparing the minimum beta limit of the $n=2$ mode (that occurs at $q_{\min}=1.45$) in Fig. 11 with Fig. 9. In Fig. 11 the minimum beta normal for the $n=2$ mode for the very flat central shear case, $\Delta q=0.005$, is $\beta_{\min}=1.9$, while in the higher reverse shear case $\Delta q=1$, $\beta_{\min}=3.2$. In Fig. 9 the minimum beta normal for the $n=2$ mode is $\beta_{\min}=1.8$ for $\Delta q=0.1$ and $\beta_{\min}=2.1$ for $\Delta q=1$. Generally, as the q profile becomes very flat, the modes with $n\geqslant 2$ become more unstable. Note the stability limit of the $n=1$ mode is only modestly affected by low central shear.

The effect of the amount of shear reversal on stability is examined in more detail in Fig. 12. Here the minimum beta limits for the $n=1$, 2, and 3 modes are plotted as a function of the amount of shear reversal. The minimum beta limit, of course, occurs at a different $q_{\min}$ value depending on the mode number. For $n=1$ the minimum beta occurs at $q_{\min}=1.9$; $n=2$, $q_{\min}=1.45$; and $n=3$, $q_{\min}=1.3$. Also shown in Fig. 12 is the maximum beta limit for the $n=1$ mode that occurs at $q_{\min}=1.2$. Starting with positive shear, as central shear is reduced the minimum beta limit rises slightly for the $n=2$ and 3 modes. As the shear is reversed the beta limit continues to rise. The beta limit rises higher for the $n=3$ mode than the $n=2$ mode, and hence negative shear appears to have a stronger stabilizing influence on higher n numbers. The amount of shear reversal, Δq, has only a modest effect on the $n=1$ mode, so that for $\Delta q>0.4$ the $n=1$ becomes the limiting instability. For equilibria with ballooning stable pressure profiles and $\Delta q>0.4$ the $n=1$ mode is the limiting MHD instability.

Next we consider the effect of pressure peaking on reverse shear equilibria that maximize beta normal and performance in TFTR. For these cases current was kept relatively high, with $q_{\text{edge}}=4.3$. In order to maximize beta, a class of ballooning stable profiles were chosen. Figure 13 shows the range of pressure profiles considered. For these profiles, Eq. (4) is used with $\alpha_0=6.0$, $b_1=-15$, $c_1=1.35$, $b_2=-2$, and $c_2=-2.0$. This creates a pressure distribution with a somewhat broader central peak. The parameter a_1 is chosen to adjust the degree of pressure peaking with $a_2=1-a_1$. In Fig. 13, two cases are shown: (1) $a_1=0.75$, resulting in the peaking factor $p_0/\langle p\rangle=4.0$; and (2) $a_1=1.0$, with $p_0/\langle p\rangle=7.2$. A value of $q_{\min}=1.2$ was chosen in order to maximize beta normal. The location of the minimum q surface was increased to $\psi_{\min}=0.3$ to allow a greater pressure gradient in the center and also increase the beta limit. In Fig. 13 both profiles are at marginal stability for the $n=1$ mode. For the peaked pressure profile case the unstable mode still peaks on the outside rational surface ($q=2$), despite the fact that p' is nearly zero there. The $n=1$ mode was found to depend primarily on global properties of the pressure profile rather than local. Several cases were tried where the location of the inner peak of the pressure profile was changed. Also, a number of cases were tried where the pressure profile was locally flattened at each and both of the mode rational surfaces. In all these cases the stability limit depended by and large only on a global measure of peakedness such as $p_0/\langle p\rangle$. Details of the pressure distribution (other than a measure of how peaked the pressure profile is) apparently have little effect on $n=1$ stability characteristics. The maximum beta normal limit as a function of the peaking factor $p_0/\langle p\rangle$ is shown in Fig. 14(a). Curves are shown for both the wall at infinity (solid line) and with a wall at the location as that in TFTR (dotted line). Similar to Fig. 7, the beta normal limit increases as the pressure profile broadens. Note that the wall has very little effect for peaked pressure profiles, but has an increasing stabilizing influence as the pressure profile broadens. This is because the $n=1$ mode has an increasing larger external component as the pressure profile is broadened. For a broad pressure distribution stable equilibria with beta normal up 3.5 are possible with no stabilizing wall present, and for a perfectly conducting wall, similar in location to that in TFTR, beta normal up to 4.1 are possible. For an ERS mode the pressure peaking factor, $p_0/\langle p\rangle$, is about 7.0. Broadening the pressure profile maximizes beta; how-

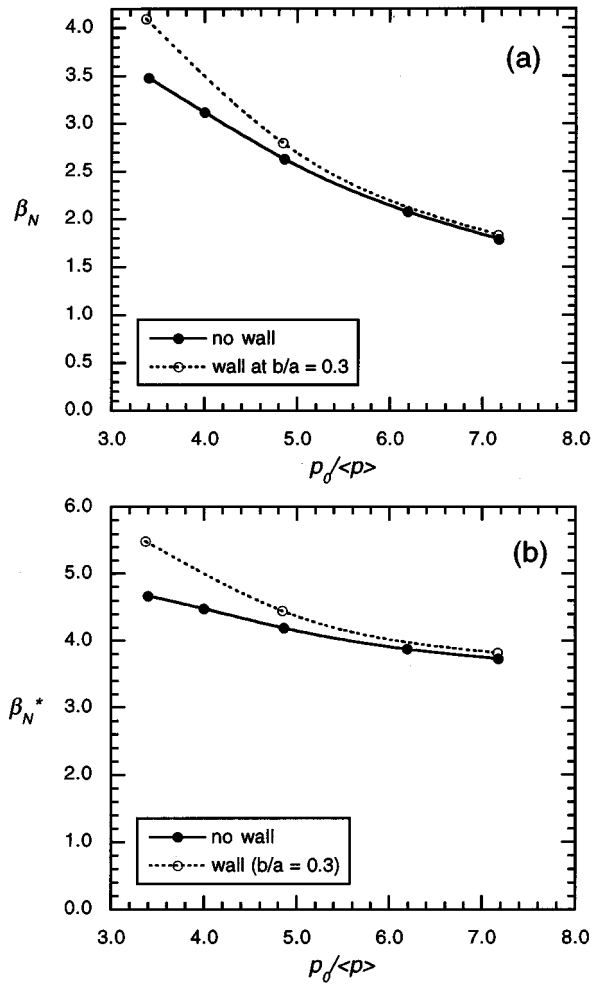

FIG. 14. Pressure peaking effects on (a) highest beta normal limit and (b) highest beta star normal limit. Here $q_{\min}=1.2$, $\Delta q=1.0$, $\psi_{\min}=0.3$, $r/a\sim 0.5$, and $q_{\text{edge}}=4.3$.

ever, as shown in Fig. 14(b), it does not have much effect on the parameter β^* where $\beta^* = 2\mu_0\sqrt{\langle p^2\rangle}/B^2$. Thermonuclear production in a fusion plasmas increases as β^* increases, and β_N^* is generally used as a good overall measure of efficiency in tokamak fusion reactor design.[23] Thus, at least for the circular case, there is little advantage to broadening the pressure profile if increasing thermonuclear production is the priority.

Figure 15 shows the effect of a perfectly conducting wall surrounding the plasma on the beta normal limits as a function of $q_{\min}$. The wall is set a constant distance from the plasma surface. The wall is somewhat less effective near rational values of $q_{\min}$, where the mode is primarily internal; however, when $q_{\min}>2$, the $n=1$ mode has a larger external component, and hence a wall can have a significant effect. Thus, wall stabilization together with reverse shear with $q_{\min}>2$ could be one possible strategy for achieving higher beta.

V. DISCUSSION

Equilibria with a reversed shear region have low-n stability properties similar in many respects to those with

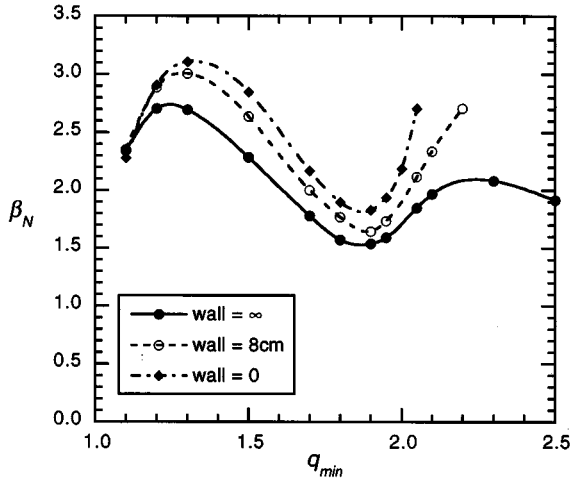

FIG. 15. The effect of perfectly conducting wall radius on the normalized beta limits for the $n=1$ instability as a function of the minimum q.

monotonic q profiles having low central shear. In both cases the main mode limiting the achievable beta is an infernal mode. The stability boundary predicted for the $n=1$ mode appears to correlate with that found experimentally during reversed shear experiments in TFTR. The stability properties of reverse shear equilibria differ from the monotonic q equilibria case in two respects: (1) moderate-n modes, $n\geqslant 2$, are more stable; and (2) the negative shear region has no critical pressure gradient imposed by ballooning modes. The lowest beta limit is set by the $n=1$ mode near $q_{\min}=2$. More reverse shear either in the form of an increased $\Delta q=q_0-q_{\min}$ or a larger shear reversal radius both tend to improve the stability limits of the $n=1$, 2, and 3 modes. A greater improvement in the beta limit occurs for the higher n modes, $n=2$ and 3. If the pressure profile is constructed so that the ballooning stability boundary is avoided, moderate-n stability boundaries are significantly higher. It is expected that the pressure profiles found in high beta experiments would tend to be of this type. Equilibria with ballooning stable pressure profiles are much more sensitive to the amount of reverse shear. For moderate-n modes increasing reverse shear tends to be more stabilizing the higher the n number—higher Δq affects $n=3$ modes more strongly than $n=2$ modes. The $n=1$ mode is the least influenced by increasing Δq. For TFTR geometry if $\Delta q>0.4$, the stability boundary is set only by the $n=1$ mode. Previously, in high-power supershots experiments beta saturates due to moderate-n MHD instabilities.[24] For supershot equilibria the beta limit for these modes is approximately at the level of the lowest beta limit of the $n=1$ mode.[15] Reverse shear offers a possible method for avoiding such instabilities and significantly increasing the beta limit achievable in the device. There are two regions that might lead to improved betas in TFTR: one low $q_{\min}$ region where $q_{\min}$ is approximately in the range $1.1<q_{\min}<1.3$, and another higher $q_{\min}$ region, where $q_{\min}>2$. If wall stabilization is effective in stabilizing the $n=1$ mode, further gains in beta are possible. Pressure peaking has a strong influence on the beta limit of the $n=1$ mode. However, in TFTR geometry it has only a

moderate to slight influence on the β^* limit. Thus, a peaked pressure distribution should produce as much fusion power output as a broad pressure distribution in circular geometry.

ACKNOWLEDGMENTS

This paper would not have been possible without the cooperation and assistance of the TFTR Physics Group. We thank them for sharing unpublished data and for the many fruitful discussions and suggestions.

This work was supported by the U.S. Department of Energy under Contract No. DEFG02-89ER51124.

[1]J. L. Luxon and L. G. Davis, Fusion Technol. **8**, 441 (1985).
[2]P. H. Rebut, J. R. Bickerton, and B. E. Keen, Nucl. Fusion **25**, 1011 (1985).
[3]E. A. Lazarus, M. S. Chu, J. R. Ferron, F. J. Helton, J. T. Hogen, A. G. Kellman, L. L. Lao, J. B. Lister, T. H. Osborne, R. Snider, E. J. Strait, T. S. Taylor, and A. D. Turnbull, Phys. Fluids B **3**, 2220 (1991).
[4]M. Hugon, B. Ph. van Milligen, S. Smeulders, L. C. Appel, D. V. Bartlett, D. Boucher, A. W. Edwards, L.-G. Eriksson, C. W. Gowers, T. C. Hender, G. Huysmans, J. J. Jacquinot, P. Kapochus, L. Porte, P. H. Rebut, D. F. H. Start, F. Tibone, B. J. D. Tubbing, M. L. Watkins, and W. Zwingmann, Nucl. Fusion **32**, 33 (1992).
[5]C. Kessel, J. Manickam, G. Rewoldt, and W. M. Tang, Phys. Rev. Lett. **72**, 1212 (1994).
[6]J. Manickam, M. S. Chance, S. C. Jardin, C. Kessel, D. Monticello, N. Pomphrey, A. Reiman, C. Wang, and L. E. Zakharov, Phys. Plasmas **1**, 1601 (1994).
[7]A. D. Turnbull, T. S. Taylor, Y. R. Lin-Lin, and H. S. John, Phys. Rev. Lett. **74**, 718 (1994).
[8]K. M. Young, M. G. Bell, W. R. Blanchard, N. L. Bretz, J. Cecchi, J. Coonrod, S. Davis, H. F. Dylla, P. C. Efthimion, R. J. Fonck, R. J. Goldston, D. J. Grove, R. J. Hawryluk, H. Hendel, K. W. Hill, J. Isaacson, L. C. Johnson, R. Kaita, R. B. Krawchuk, R. Little, M. McCarthy, D. McCune, K. McGuire, D. Meade, S. S. Medley, D. Mikkelsen, D. Mueller, E. Nieschmidt, D. K. Owens, A. Ramsey, A. L. Roquemore, L. Samuelson, N. Sauthoff, H. Park, J. Schivell, J. A. Schmidt, S. Sesnic, J. Sinnis, J. Strachan, G. D. Tait, G. Taylor, F. Tenny, and M. Ulrickson, Plasma Phys. Controlled Fusion **26**, 11 (1984).
[9]J. D. Strachan, M. Bitter, A. T. Ramsey, M. C. Zarnstorff, V. Arunasalam, M. G. Bell, N. L. Bretz, R. Budny, C. E. Bush, S. L. Davis, H. F. Dylla, P. C. Efthimion, R. J. Fonck, E. Fredrickson, H. P. Furth, R. J. Goldston, L. R. Grisham, B. Grek, R. J. Hawryluk, W. W. Heldbrink, H. W. Hendel, K. W. Hill, H. Hsuan, K. P. Jaehnig, D. L. Jassby, F. Jobes, D. W. Johnson, L. C. Johnson, R. Kaita, J. Kamperschroer, R. J. Knize, T. Kozub, H. Kugel, B. LeBlanc, F. Levinton, P. H. La Marche, D. M. Manos, D. K. Mansfield, K. McGuire, D. H. McNeill, D. M. Meade, S. Sedley, W. Morris, D. Mueller, E. B. Nieschmidt, D. K. Owens, H. Park, J. Schivell, G. Schilling, G. L. Schmidt, S. D. Scott, S. Sesnic, J. C. Sinnis, F. J. Stauffer, B. C. Stratton, G. D. Tait, G. Taylor, H. H. Towner, M. Ulrickson, S. von Goeler, R. Wieland, M. D. Williams, K.-L. Wong, S. Yoshikawa, K. M. Young, and S. J. Zweben, Phys. Rev. Lett. **58**, 1004 (1987).
[10]F. M. Levinton, M. C. Zarnstorff, S. H. Batha, M. Bell, R. E. Bell, R. V. Budny, C. Bush, Z. Chang, E. Fredrickson, A. Janos, J. Manickam, A. Ramsey, S. A. Sabbagh, G. L. Schmidt, E. J. Synakowski, and G. Taylor, Phys. Rev. Lett. **75**, 4417 (1995).
[11]F. M. Levinton, R. J. Fonck, G. M. Gammel, R. Kaita, H. W. Kugel, E. T. Powell, and D. W. Roberts, Phys. Rev. Lett. **63**, 2060 (1989).
[12]S. P. Hirshman, D. K. Lee, F. M. Levinton, S. H. Batha, M. Okabayashi, and R. M. Wieland, Phys. Plasmas **1**, 2277 (1994).
[13]J. Delucia, S. C. Jardin, and A. M. M. Todd, J. Comput. Phys **37**, 1983 (1980).
[14]A. Brandt, Math. Comput. **31**, 333 (1977).
[15]R. V. Budny, Nucl. Fusion **34**, 1247 (1994).
[16]M. D. Kruskal and C. R. Oberman, Phys. Fluids **2**, 23 (1959).
[17]M. H. Hughes, M. W. Phillips, and R. G. Storer, Comput. Phys. Commun. **72**, 76 (1992).
[18]J. Manickam, N. Pomphrey, and A. M. M. Todd, Nucl. Fusion **27**, 1461 (1987).
[19]M. H. Hughes, M. W. Phillips, and E. D. Fredrickson, Phys. Fluids B **5**, 3267 (1993).
[20]F. Troyon, R. Gruber, Phys. Lett. A **110**, 29 (1985).
[21]J. R. Ferron, M. S. Chu, F. J. Helton, W. Howl, A. G. Kellman, L. L. Lao, E. A. Lazarus, J. R. Lee, T. H. Osborne, E. J. Strait, T. S. Taylor, and A. D. Turnbull, Phys. Fluids B **2**, 1280 (1990).
[22]R. J. Hastie and J. B. Taylor, Nucl. Fusion **21**, 187 (1981).
[23]R. C. Davidson, R. J. Goldston, G. H. Neilson, and K. I. Thomassen, Phys. Plasmas **2**, 2417 (1995).
[24]E. D. Fredrickson, V. Arunasalem, C. W. Barnes, M. Bell, M. Bitter, H. S. Bosch, N. L. Bretz, R. V. Budny, C. Bush, A. Cavallo, L. Chen, C. Z. Cheng, T. K. Chu, S. A. Cohen, P. Colestock, D. Coster, D. L. Dimock, H. F. Dylla, P. C. Efthimion, A. Ehrhardt, R. J. Fonck, H. P. Furth, G. Gammel, R. J. Goldston, G. Greene, B. Grek, L. Grisham, G. Hammet, R. J. Hawryluk, H. W. Hendel, K. Hill, E. Hinnov, S. P. Hirshman, J. Hosea, B. Howell, H. Hsuan, R. Hulse, A. C. Janos, D. Jassby, D. Johnson, R. Kaita, C. Kieras-Phillips, S. J. Kilpatrick, V. A. Krupin, P. H. LaMarche, B. LeBlanc, R. Little, A. I. Lysoyvan, D. M. Manos, D. Mansfield, E. Mazzucato, D. McCarthy, D. C. McCune, K. M. McGuire, D. H. McNeill, D, Meade, D. R. Mickelsen, A. D. Monticello, R. Motley, S. S. Medley, D. Mueller, J. Murphy, Y. Murakami, D. K. Owens, H. K. Park, W. Park, A. Ramsey, M. H. Redi, T. Saito, G. Schilling, J. Schivell, G. L. Schmidt, S. D. Scott, J. C. Sinnis, B. C. Stratton, W. Stodiek, E. J. Synakowski, G. Taylor, H. H. Towner, M. Ulrickson, S. von Goeler, R. M. Weiland, R. White, J. R. Wilson, K. M. Young, M. C. Zarnstorff, and S. Zweben, in *Plasma Physics and Controlled Nuclear Fusion Research*, Proceedings of the 13th International Conference, Washington, DC, 1990 (International Atomic Energy Agency, Vienna, 1991), Vol. I, p. 559.